On the origin of chevron marks and striated grooves, and their use in predicting mud bed rheology

McGowan, Dylan; Salian, Amisha; Baas, Jaco; Peakall, Jeff; Best, Jim

Sedimentology

DOI:
10.1111/sed.13148

Published: 01/02/2024

Peer reviewed version

SEDIMENTOLOGY
the journal of the
International Association of Sedimentologists

On the origin of chevron marks and striated grooves, and their use in predicting mud bed rheology

Journal:	*Sedimentology*
Manuscript ID	SED-2022-OA-235.R2
Manuscript Type:	Original Article
Date Submitted by the Author:	18-Sep-2023
Complete List of Authors:	McGowan, Dylan; Bangor University, School of Ocean Sciences Salian, Amisha; Bangor University, School of Ocean Sciences Baas, Jaco; Bangor University, School of Ocean Sciences Peakall, Jeff; University of Leeds, Earth and Environment Best, Jim; University of Illinois at Urbana-Champaign, Geology
Keywords:	continuous tool marks, groove marks, striations, chevron marks, physical experiments, bed density, yield stress

On the origin of chevron marks and striated grooves, and their use in predicting mud bed rheology

Dylan McGowan[1], Amisha Salian[1], Jaco H. Baas[1], Jeff Peakall[2], Jim Best[3]

[1] School of Ocean Sciences, Bangor University, Menai Bridge, LL59 5AB, Wales, UK

[2] School of Earth and Environment, University of Leeds, Leeds, LS2 9JT, UK

[3] Departments of Earth Science and Environmental Change, Geography and GIS, and Mechanical Science and Engineering and Ven Te Chow Hydrosystems Laboratory, University of Illinois at Urbana-Champaign, Urbana 61801, USA

KEYWORDS: continuous tool marks; groove marks; striations; chevron marks; physical experiments; bed density; yield stress

ABSTRACT

Understanding of the formative conditions of many sole structures is limited, with chevron marks and striated groove marks being particularly enigmatic. Herein, we examine these sedimentary structures through laboratory modelling. An idealised tool, resembling an armoured mud clast, was dragged through substrates of kaolinite–seawater mixtures of different yield strengths while submerged in seawater. The experiments suggest that armoured mud clasts are the likely tools producing fine striae in striated grooves, and, given the common occurrence of striated groove marks in outcrops, that these clasts are more prevalent in deep-marine settings than previously thought. Chevron marks were observed to form over a narrow range of substrate yield stresses, likely explaining their relative rarity. Furthermore, their form is shown to be a function of substrate rheology, with chevron angle relative to the movement direction of the tool being less in weaker substrates. Moreover, the size of cut chevron marks, characterised by a narrow central cut, bears no relationship to the size of the incising tool, but rather reflects a substrate with a low yield stress that is sufficiently mobile to close behind the tool. In contrast,

interrupted chevron marks, characterised by a distinct central groove, reflect greater substrate strength. Striated grooves without chevrons formed at the highest yield stresses simulated in the experiments. The relationship between tool mark type and yield stress, in combination with changes in chevron angle, enables these sole structures to be utilised as indicators of palaeosubstrate rheology. The conditions required to preserve such features include a prolonged period of bed consolidation, flow bypass, and lack of bioturbation. Given changes in seafloor communities and bioturbation over time and their impact on substrate rheology, particularly during the early Palaeozoic, the present work supports the idea that the frequency of these sole structures likely changed over geological time.

INTRODUCTION

Sole marks are erosional sedimentary structures formed by the interaction of a flow, or an object present at or near the base of the flow, with a sediment bed, usually consisting of cohesive mud (Dżułyński & Sanders, 1962; Collinson *et al.*, 2006). Their common occurrence and predictable orientation relative to the direction of the flow, or the moving object, has secured sole marks as a prime indicator of palaeoflow direction and orientation in the sedimentary record (*e.g.*, Hall, 1843). More recently, the shape and size of sole marks have been linked with specific types of formative clay-laden flows (Peakall *et al.*, 2020), where: (i) turbulent and turbulence-enhanced flows (*sensu* Baas & Best, 2002; Baas *et al.*, 2009) form scour marks, such as flute marks; (ii) turbulence-attenuated flows form mainly discontinuous tool marks, such as prod marks and skim marks, and; (iii) quasi-laminar plug flows (*sensu* Baas *et al.*, 2009) and fully laminar plug flows (Peakall *et al.*, 2020) generally form continuous tool marks, such as groove marks and chevron marks. However, the formative conditions for many sole structures remain poorly constrained, particularly for chevron marks and striated grooves. Peakall *et al.* (2020) postulated a mechanism for the formation of striated grooves and suggested that the internal striae are formed by clast asperities or potentially armoured mud clasts. Chevron marks have been attributed to shear stress imposed by flows above weak, ductile muds (Dżułyński & Walton, 1965) and the formation of wakes generated around the object, with analogies made to 'bow waves' formed by ships. This link to weak, ductile muds suggests that shape and size of chevron marks are a function of substrate properties.

The process-orientated conceptual model of Peakall *et al.* (2020) has been applied to outcrop studies (*e.g.*, Baas *et al*., 2021; Postma *et al.*, 2021; Brooks *et al.*, 2022), but the role of substrate control on sole mark development, and, specifically, the shape and size of striated groove and chevron marks, remains poorly understood. In general, the erodibility of a substrate, and therefore the formation of sole marks, depends on a multitude of physical, chemical, and biological factors (Peakall *et al.*, 2020). These include the shape and size of the impacting tool and the bed properties of mean grain size and size distribution, plasticity index, bulk density, water content, organic matter content, clay mineralogy, bioturbation, concentration of extracellular polymeric substances, and early diagenetic cements. Even though all these factors combine to govern erodibility, bulk density — closely related to water content in mud — exerts the dominant control on erosion in cohesive substrates (Amos *et al.*, 2004; Winterwerp *et al.*, 2012). Here, erodibility is approximated by the yield stress of the substrate, rather than by bed density, because yield stress is independent of clay type. We hypothesise that yield stress governs the shape and size of specific sole marks, and, conversely, that sole marks in sedimentary rocks provide information on the erodibility of the muddy bed during the formation of sole marks. Sole marks may thus present an indirect measure for the rheological characteristics of muddy substrates that is difficult to obtain otherwise.

In the present paper, the above-mentioned hypotheses are tested through a series of controlled laboratory experiments using an artificial 'armoured' clast, where the rheology of the bed was altered to assess the role of the substrate on the formation of sole structures. The aims of this paper are to: (1) investigate the effect of mud bed rheology on the formation and preservation state of continuous tool marks; (2) determine the formation mechanism of striated groove marks; (3) delimit the rheological properties of the bed, necessary for the generation and preservation of continuous tool marks, and; (4) determine how the experimental data can be used as a means for interpreting the rheology of muddy substrates in the geological record from the type, size, and shape of continuous tool marks.

BACKGROUND

Chevron marks and groove marks are continuous tool marks, as opposed to discontinuous tool marks, such as skim and prod marks (Dżułyński & Sanders, 1962; Peakall *et al.*, 2020). Continuous, often straight, tool marks generally

extend beyond the scale of outcrops, as shown by 35-m long groove marks described by Draganits *et al.* (2008). In deep-marine environments, these marks are formed by tools, commonly mud clasts that are carried by the flow (Peakall *et al.*, 2020), whilst in shallow water a wider range of tools is inferred, including woody debris (Lamb *et al.*, 2008; Myrow *et al.*, 2008). The nature of these structures and their proposed formative mechanisms are reviewed briefly here.

Chevron marks

Viewed in planform, chevron marks consist of closely-spaced V- or U-shaped ridges that close in the direction of travel (Fig. 1; Dżułyński & Sanders, 1962). Chevron marks can possess V-shaped ridges separated by a central cut (cut chevrons) or groove (interrupted chevrons), or V- or U-shaped ridges that lack any central lineation (uninterrupted chevrons; Figs 1 and 2; Craig & Walton, 1962; Dżułyński & Sanders, 1962). Cut and interrupted chevrons have been linked to a tool that cuts into the substrate, whilst uninterrupted chevrons have been postulated to form from a tool that is not in contact with the bed, but travels at a fixed height above the bed (Dżułyński & Walton, 1965; Peakall *et al.*, 2020). Chevrons are generally narrow, a few millimetres wide (Fig. 2C), although larger widths in the centimetric range are associated with interrupted chevrons (Figs 2B, D). Some chevrons, particularly of centimetric width, may show a distinctive pattern with the downstream end of the ridge being steepest, and folded over on itself (Figs 1 and 3). Although the relative frequency of chevrons has not been documented in the literature, our observations from extensive fieldwork examining sole marks, is that they are comparatively rare, with just a few observed across whole field areas (*e.g.*, Aberystwyth Grits, Wales, Baas *et al.*, 2021).

Experiments dragging a stick through mud, or a matchstick above a mud bed, generated cut chevrons and uninterrupted chevrons, respectively (Dżułyński & Walton, 1963, 1965; Kelling *et al.*, 2007). Similarly, experiments with plaster-of-Paris flows over weak mud beds, and sand-rich flows over plaster-of-Paris beds, enabled tools to form chevron marks (Dżułyński & Walton, 1963; Dżułyński & Simpson, 1966; Dżułyński, 1996). However, these experiments lacked data on flow and bed rheology, and the authors were unable to elucidate formative mechanisms. In the absence of experimental evidence, there has been debate concerning the mechanisms forming chevron marks. Chevrons have been postulated to form from the shear stress imposed by flows on weak, ductile muds, because of wakes that are analogous to those generated behind ships (Craig & Walton, 1962; Dżułyński &

Sanders, 1962). Ships form interrupted chevrons in water, as the ship cuts through the bow wave. Later, Dżułyński & Walton (1965) argued that, if a tool cuts the bed, the sediment to the side may form ridges. The exact mechanism, whether physical or fluidal, for creating ridges was not described, although it can be assumed to be fluidal, based on the work of Craig & Walton (1962) and Dżułyński & Sanders (1962). The formative mechanics of uninterrupted chevrons have been debated by Dżułyński & Walton (1965), Allen (1984) and Peakall *et al.* (2020). Dżułyński & Walton (1965) argued for eddying behind a tool, with reduced suction on the substrate as the particle moves away from the bed. In turn, Dżułyński & Walton (1965) posited that this led to a change from V-shaped to U-shaped chevrons. However, Allen (1984) argued that this mechanism was untenable as the tool should travel at a slower rate than the flow, and thus any eddies should advect downstream, not upstream as interpreted from the chevron direction. If, as argued by Peakall *et al*. (2020), the tools are supported in the base of a plug flow, the objections of Allen (1984) are overcome, as the tool travels at the same speed as the flow.

Striated grooves

Grooves in deep-marine systems, where they were initially defined, are remarkably straight, although some gently curve, exhibit constant width and depth, and are typically continuous on the scale of an individual outcrop. Some of these are associated with raised ridges on their flanks (Dżułyński & Walton, 1965), but their margins are typically sharp. Grooves may also possess parallel striae (Dżułyński & Walton, 1965; Allen, 1984; Fig. 2E). Groove widths range from millimetric to several metres and groove depths extend from several millimetres to *c.* 200 mm (Dżułyński & Walton, 1965; Draganits *et al*., 2008). Few data have been collated on the internal striae of grooves. However, up to tens of striae, with typically millimetric to centimetric spacing, are shown in photographic examples (Peakall *et al*., 2020; Fig. 2E). In shallow-marine environments, grooves have been defined differently, to include continuous examples, but also shorter, discontinuous features (*e.g.,* Benton & Gray, 1981; Beukes, 1996; Lamb *et al*., 2008), referred to as bounce or skim marks in the deep-marine literature (Dżułyński & Sanders, 1962; Allen, 1984; Peakall *et al.*, 2020) and sedimentological textbooks (Bridge & Demicco, 2008; Boggs, 2014; Collinson & Mountney, 2019). We herein use the original deep-marine definition for grooves.

The formation of grooves has been linked to the dragging of tools through a cohesive substrate. However, the nature of the formative flows has remained enigmatic, with a wide range of different flow conditions postulated. Peakall *et al*. (2020) reviewed the formative mechanisms for grooves, and concluded that their constant width, depth, and straightness demonstrate that the tools must have been held rigidly at a constant height, without undergoing rotation, which in turn indicates a flow with cohesive strength. Peakall *et al*. (2020) proposed that grooves were formed by debris flows, or in some cases slumps and slides, with the tools held rigidly to the base of the plug flow. Specifically, grooves were associated with quasi-laminar plug flows or laminar plug flows (Baas *et al*., 2009; Peakall *et al*., 2020), with Peakall *et al.* (2020) suggesting that striated grooves might be the product of clast asperities or armoured mud clasts.

Pristine preservation of chevron marks and striated grooves

The pristine preservation of chevrons and often millimetric striae in outcrops (*e.g.*, Fig. 2; Peakall *et al*., 2020) raises a paradox: How does a flow that transports a tool in a fixed position and drags it through the substrate, not erode these millimetric structures, once formed? Herein, we present a new model for the structure of, and the position of tools in, these formative flows that resolves this paradox.

METHODS

The formation of tool marks was modelled in the Hydrodynamics Laboratory of the School of Ocean Sciences, Bangor University, by dragging an object submerged in seawater across a muddy substrate in a rectangular tank, 0.115 m wide, 0.674 m long, and 0.153 m high (Fig. 4; Video 1). The tank was filled up to half its height (*c.* 0.076 m) with a homogeneous mixture of kaolin clay (Whitchem China Clay Polwhite E Powder; median grain size: 0.009 mm; density, ρ_s: 2600 kg m^{-3}) and seawater (density, ρ_w: 1027 kg m^{-3}). After flattening the clay surface, seawater was added to a height of *c.* 0.14 m. The seawater was sourced from the Menai Strait, a tidal channel next to the Hydrodynamics Laboratory, and was filtered to remove suspended material before being used in the experiments. Twelve experiments were conducted using bed bulk densities ranging from 1367.7 kg m^{-3} to 1612.2 kg m^{-3} (Table 1), equivalent to water contents ranging from 62.8% to 78.3%. At bed densities below 1300 kg m^{-3}, or a water content above 83%, the substrate was unstable because of high rates of consolidation and dewatering.

Herein, the yield stress, which is the minimum shear stress required to initiate motion of a clay–water mixture, is used to describe the cohesive strength of the clay beds. Using yield stress instead of bed bulk density removes the need to consider clay type, because, for example, kaolinite is less cohesive than illite at a given concentration in the sediment bed (Hillel, 2004; Yong *et al.*, 2012). Amongst the clay minerals most commonly found in nature, kaolinite is the weakest whilst montmorillonite is the strongest in terms of cation exchange capacity, a parameter used commonly to describe cohesion (*e.g.*, Baker *et al.*, 2017). Baker *et al.* (2017) measured the yield stress of kaolinite and montmorillonite (bentonite), using the same type of kaolinite from the same supplier as in the present experiments (Whitchem China Clay Polwhite E Powder). Using data from Baker *et al.* (2017; table 2), the following best-fit equations were derived for kaolinite (Equation 1) and montmorillonite (Equation 2):

$$\tau_y = 3.1 \cdot 10^{-3} C^{3.15} \quad (1)$$

$$\tau_y = 6 \cdot 10^{-3} C^{3.05} \quad \text{for } C \leq 18\% \quad (2a)$$

$$\tau_y = 90.5C - 1588 \quad \text{for } C > 18\% \quad (2b)$$

where τ_y is the yield stress and C is the percentage volumetric clay concentration, which can be converted from bed density, ρ_b, using:

$$C = 100\frac{\rho_b - \rho_w}{\rho_s - \rho_w} \quad (3)$$

where ρ_w = 1027 kg m^{-3} is the density of seawater and ρ_s is the sediment density: ρ_s = 2600 kg m^{-3} for kaolinite and ρ_s = 2350 kg m^{-3} for montmorillonite. Equations 1–3 were used to show that the range of bed bulk density used in the present experiments (1367.7 kg m^{-3} to 1612.2 kg m^{-3}) corresponds to yield stresses of 50.0 N m^{-2} to 274.7 N m^{-2}, and that the bed was unstable at 1300 kg m^{-3} equivalent to τ_y < 24.9 N m^{-2}. In turn, these yield stresses correspond to bulk bed densities of montmorillonite–seawater mixtures of 1266.5 kg m^{-3} to 1299.3 kg m^{-3}, with instability below 1230.0 kg m^{-3}.

Van Rijn (1993) proposed a classification scheme for natural clay beds based on density limits (Table 2), which is used herein to nominally describe the clay beds. Given the arguments above, it would be more generically useful to define bed types based on yield stress limits. Beds composed of mixtures of different clay mineral types, which include moderately cohesive illite, are more typical in the natural environment than beds composed solely of weakly cohesive kaolinite or strongly cohesive montmorillonite (Baker *et al.*, 2017). As a first approximation, and in the

absence of further relevant data, we therefore take the average bed densities for kaolinite and montmorillonite to convert the bed density limits of van Rijn (1993) to yield stress limits (Table 2). This reveals that the experiments mainly covered 'fluid–solid' and 'stiff mud' bed types, which, according to the estimations of van Rijn (1993), take on the order of a year to decades to form by consolidation of a fluid mud (Table 2).

The object used in the experiments was a hollow spikey ball filled with wet sand (Fig. 5). The ball had a mass of 0.1185 kg and diameter of 0.052 m (volume: 7.5 x 10^{-5} m^3), and the spikes were 6.5 mm long and 5 mm wide. The ball was placed on the sediment surface and allowed to penetrate the bed under its own weight, and then attached to a fishing reel by means of a thin wire attached to a threaded bolt (Fig. 4), to allow the ball to be dragged manually across the muddy bed at a near-constant dragging speed of 54 ± 16 mm s^{-1}. Each experiment lasted *c*. 13 seconds, with the choice of velocity allowing the clast to stay in continual contact with the bed. Before commencing each experiment, a small amount of brown bentonite clay was sprinkled in transverse bands onto the white kaolin surface in order to visualise bed deformation caused by movement of the object (Fig. 4). Exceptions were experiments with yield stresses of 50.0 N m^{-2}, 69.1 N m^{-2}, and 91.3 N m^{-2}, in which the bentonite was sprinkled onto the bed uniformly, rather than in distinct bands. After each experiment, the seawater was siphoned out of the tank at a rate slow enough to prevent bed disturbance. Thereafter, the shape and size of the tool mark were recorded using a protractor and calliper gauge. The calliper gauge was also used to record a vertical profile of the tool mark perpendicular to the dragging direction at a horizontal and vertical resolution of 5 mm and 0.1 mm, respectively.

RESULTS

Visual observations of tool mark development and tool mark shape and size

The experimental data reveal considerable changes in tool mark formation mechanism, shape and size, as the yield stress was increased and the bed type changed from fluid mud to stiff mud. These changes were recorded in four different types of tool mark (Fig. 6): (1) wide, low-angle chevron marks with a narrow, central, non-striated groove (Fig. 6A); (2) striated groove marks with pronounced low-angle chevron marks and surficial clay clasts (Figs 6B, C); (3) striated groove marks with narrow, medium- to high-angle chevron marks (Figs 6D, E), and; (4) striated groove marks without chevron marks (Fig. 6F). Before describing each of these types and their formative mechanism in

detail, it should be noted that the spherical tool produced tool marks only at yield stresses >58.9 N m^{-2}. As mentioned previously, the bed was unstable at <24.9 N m^{-2}, because of high rates of consolidation. A more stable gel developed between 24.9 N m^{-2} and 58.9 N m^{-2}, but these yield stresses were too low to support the tool, which was then largely, or fully, submerged below the bed surface.

Wide, low-angle chevron marks with a narrow, central, non-striated groove (cut chevron marks)

Between yield stresses of 58.9 N m^{-2} and 71.6 N m^{-2}, roughly half of the tool was submerged below the bed surface before it was dragged across the bed. During dragging, clay was displaced sideways and over the top of the tool. Most of this clay filled the groove formed by the moving tool immediately, thus preserving a shallow and narrow groove, up to 5 mm deep and 6 mm wide (Figs 6A and 7A). This groove lacked striae and possessed chevrons that were formed by ductile deformation of the clay away from the surface of the moving tool (Fig. 6A). These chevrons stretched across the entire width of the tank and their angle with respect to the dragging direction was 34°.

Striated groove marks with low-angle chevrons and surficial clay clasts (low-angle interrupted chevron marks)

Combined groove–chevron marks were formed at yield stresses between 71.6 N m^{-2} and 82.8 N m^{-2} (Figs 6B, C). The grooves were wider than the local diameter of the tool at the point where it was cutting the bed, because the side walls of the grooves collapsed behind the moving tool, helped by the large initial depth and steep walls of the grooves (Figs 7B, C). The collapsed sediment was preserved as clay clasts lining the wall of the grooves (Figs 6B, C). These tool marks possessed lateral ridges, up to 5 mm high (Figs 7B, C), formed by accumulation of clay pushed sideways by the moving tool. In contrast to the cut chevron marks, no clay was pushed over the top of the tool and the clay was too cohesive to fill the groove behind the moving tool, except as clasts. The spikes on the spherical tool formed parallel striae in the grooves, but these were partially covered by the clay clasts (Figs 6B, C). The chevrons were similar to those in the cut chevron marks, except for a smaller angle relative to the dragging direction: 25° and 16° at yield stresses of 74.4 N m^{-2} and 79.9 N m^{-2}, respectively. These tool marks are therefore categorised as low-angle interrupted chevron marks.

Striated groove marks with narrow, medium- to high-angle chevrons (high-angle interrupted chevron marks)

These tool marks, which formed at yield stresses between 82.8 N m^{-2} and 158.0 N m^{-2}, were similar to the low-angle interrupted chevron marks, but with notable differences. The chevron angle rapidly increased as the yield stress

increased (Figs 6D, E), culminating in an 84° angle, *i.e.,* an almost total lack of chevrons, at 143.7 N m^{-2}. These tool marks are therefore categorised as high-angle interrupted chevron marks. The chevrons narrowed as chevron angle increased, until their width was less than 10 mm at a yield stress of 143.7 N m^{-2}. The striae in the grooves of the high-angle interrupted chevron marks were not covered by clay clasts, and thus the continuous character and sharpness of individual striae were better exposed, when viewed from above (Figs 6D, E). The grooves were also narrower and shallower, and their lateral ridges thinner, than those of the low-angle interrupted chevron marks (Figs 7D–G).

Striated groove marks without chevrons (chevron-less groove marks)

These tool marks, formed at yield stresses between 158.0 N m^{-2} and 274.7 N m^{-2}, were chevron-less groove marks, with small groove widths and shallow groove depths (Figs 6F and 7H–J). These characteristics reflect the shallow initial penetration depth of the tool into these firm substrates. Striae in the groove marks were sharp and perfectly parallel (Fig. 6F), and the lateral ridges had a thickness similar to those in the high-angle interrupted chevron marks.

Geometrical characterization of the tool marks

Characteristic geometrical properties of the experimental tool marks are plotted against yield stress in Fig. 8. Figure 8A shows the maximum depth of the grooves and the mean of the maximum thickness of the left-lateral and right-lateral ridges lining the grooves. The maximum depth increased rapidly from 5 mm to 15.5 mm across the boundary between the cut, and low-angle interrupted, chevron marks (Fig. 8A), which was associated with the change from filling of the groove behind the moving tool at τ_y = 69.1 N m^{-2} to unfilled grooves. The low-angle interrupted chevron marks were the deepest of all the tool mark types, with the groove depth of the high-angle interrupted chevron marks gradually decreasing linearly as yield stress increased (Fig. 8A). This trend continued for the chevron-less groove marks, but at a slower rate than for the high-angle interrupted chevron marks. The chevron-less groove marks were only 0.6 mm to 2.7 mm deep (Fig. 8A).

The cut chevron marks lacked lateral ridges (Figs 7A and 8A), whereas the deep low-angle interrupted chevron marks had well-developed lateral ridges with a maximum thickness of 3.5 mm and 4.9 mm on each of the two flanks. The shallower, high-angle, interrupted chevron marks and chevron-less groove marks lacked clear trends in lateral ridge thickness (Fig. 8A). The mean thickness for these tool marks was *c.* 2 mm, which is *c.* 50% of the low-

angle interrupted chevron mark thickness. Lateral ridges were absent at the highest yield stress of 274.7 N m^{-2} (Fig. 8A).

Groove mark width (Fig. 8B) shows a proportional relationship to groove mark depth (Fig. 8A); wide groove marks tended to be deep, and narrow groove marks tended to be shallow. Hence, the cut chevron marks had the lowest width, the low-angle interrupted chevron marks had the highest width, and there is an inverse relationship between groove mark width and yield stress for the high-angle interrupted chevron marks and chevron-less groove marks (Fig. 8B). The angle of the chevrons with respect to the tool dragging direction changed with yield stress (Fig. 8C). These angles decreased from 34° to 25° to 16° across the boundary between the cut and low-angle interrupted chevron marks. The low angles of the latter correspond to the large groove depths and widths, and thick lateral ridges of this tool mark type. The high-angle interrupted chevron marks possessed narrower chevrons, with angles that increased from 59° to 84°, as yield stress increased. The bentonite bands were not deformed in the chevron-less groove marks (shown by the 90° angles in Fig. 8C).

DISCUSSION

Origin of chevron marks and striated groove marks

General remarks

The experimental data support the previous concept that tools dragged across a soft, muddy substrate can form cut chevron marks (Fig. 6A) and interrupted chevron marks (Figs 6B–E) (Dżułyński & Walton, 1963, 1965; Dżułyński & Simpson, 1966; Dżułyński, 1996; Kelling *et al*., 2007) and that striated grooves are the product of clasts with asperities (Figs 6B–F; Peakall *et al*., 2020). Uninterrupted chevron marks did not form in the experiments, suggesting that these features are not related to tools cutting the bed. These may instead be related to tools dragged above the bed, as postulated since the 1960s (Craig & Walton, 1962; Dżułyński & Sanders, 1962).

Origin of chevron marks

The present experiments provide novel information concerning the formative mechanisms of cut and interrupted chevron marks as influenced by differences in yield stress of the clay. These improve upon earlier experiments

conducted with plaster-of-Paris, for which the yield stresses were not measured (Dżułyński & Walton, 1963; Dżułyński & Simpson, 1966; Dżułyński, 1996). Chevrons formed only in the kaolinite beds at τ_y = 58.9 – 158.0 N m^{-2}. The chevron marks with a narrow, central groove resemble cut chevron marks, whereas the groove marks with variably angled chevrons resemble interrupted chevron marks (*cf.*, Dżułyński & Walton, 1963, 1965; Dżułyński & Simpson, 1966; Dżułyński, 1996; Kelling *et al*., 2007). The present experiments show that the cut chevron marks, which formed at a narrow range of yield stresses between 58.9 N m^{-2} and 71.6 N m^{-2}, require water-rich clay beds with a relatively low cohesive strength. We infer that the shear induced by the moving tool was able to deform, re-orientate, and possibly also break the bonds between the kaolinite particles (*cf.*, Philippe *et al.*, 2011). This caused the displaced kaolinite to move around and over the top of the tool like a fluid, quickly filling the groove behind the tool, and preserving the original groove as a shallow, narrow structure. Additionally, more ductile deformation caused the formation of chevron marks away from the centre of shear around the tool, where the clay structure remained largely intact. This stressing of the ductile clay adjacent to the moving tool (Craig & Walton, 1962; Dżułyński & Sanders, 1962) created wide chevrons that extended to the walls of the tank. The low angle of the cut chevron marks is a further indication of the highly ductile properties of the kaolinite–water mixture under these experimental conditions.

The interrupted chevron marks, which formed at τ_y = 71.6 – 158.0 N m^{-2}, had wider and generally deeper grooves than the cut chevron marks, because the grooves were not infilled with kaolinite that was pushed sideways and backward by the moving tool, as present in the cut chevron marks. Instead, the clay accumulated predominantly onto lateral ridges (Figs 7B–G; Dżułyński & Walton, 1965). The presence of these lateral ridges, together with the presence of mud clasts that lined the deep grooves, suggests that the cohesive bed strength associated with interrupted chevron marks is greater than for cut chevron marks. However, the low-angle interrupted chevron marks were still sufficiently ductile to form low-angle chevrons that extended to the walls of the tank. In contrast, the high-angle interrupted chevron marks attained a progressively greater chevron angle (Fig. 8C), and a narrower width, as a result of an increase in the yield stress from 82.8 N m^{-2} to 158.0 N m^{-2}. These trends are likely because bed deformation at these higher yield stresses decays more quickly away from the moving tool, and possibly because the tool did not penetrate as deeply into the bed, thus reducing the total amount of shear. The cohesive strength of the bed at yield stresses >158.0 N m^{-2} was too great to allow the formation of chevrons, thus generating

chevron-less groove marks. The stability field of these groove marks probably extends beyond the maximum yield stress of 274.7 N m^{-2} investigated herein, although it is likely there is a yield strength above which the bed is too hard to form grooves and their striae. Further research is needed to establish this limit for kaolinite and other clay types, and possibly other tool shapes.

Returning to the analogy between chevrons and ship wakes, we note that deep-water ship wakes have a constant angle of 19.5° (Bertram, 2000), close to the minimum angle observed herein for the striated groove marks with pronounced low-angle chevrons (Fig. 8C). In shallower water, ship wake angles increase to up to 90° at a Froude number, $Fr = U/\sqrt{(gh)} = 1$, where U is ship velocity, g is the gravitational constant and h is the water depth, before progressively decreasing again in supercritical conditions ($Fr > 1$; Bertram, 2000). The experimental chevron angles are more analogous to these shallow-water examples of ship wakes than those of ship wakes in deep water. Therefore, chevron mark angle may also be a function of velocity, a parameter not examined in the present study.

Nature of the formative tools in striated grooves

Except for the narrow grooves of the cut chevron marks, striae were preserved and straight (*cf.*, Peakall *et al.*, 2020) in all the grooves. Hence, the formation and preservation of striated grooves is independent of yield stress, provided that the bed can be deformed in a ductile manner. However, striae are particularly well-defined in chevron-less groove marks formed in stiff, high-yield-stress clay, and they are partly covered by mud clasts at the edge of grooves in low-angle interrupted chevron marks.

The present experiments therefore demonstrate that tools with asperities form striated grooves, but a key question is what types of tools form striated groove marks in nature? The thin delicate nature of some internal striae, and the large number of striae — typically tens of striae — observed in some outcrop cases, would appear to require an unusual number, and tight spacing, of sharp asperities on the surface of the formative tools. In some cases, striae also appear regularly spaced (Fig. 2E). It is hard to envisage how primary unlithified mud clasts that dominate tools in deep-marine environments (Peakall *et al*., 2020) would exhibit this range of features on account of their initial erosion, or how, if present, such sharp and frequently small asperities would avoid breakage and abrasion during dragging of the clast through the substrate. In shallow-marine environments, woody debris is also unlikely to exhibit such sharp and frequent asperities. Tools comprised of strong asperities that would restrict breakage and abrasion

might include diagenetically-produced features such as concretions (*e.g.*, Loope *et al*., 2012; Pe-Piper & Piper, 2020), and armoured mud clasts that roll over a surface whilst acquiring a coating of granular bed material (Li *et al*., 2017), which would provide the asperities. Concretions are typically smooth, although in exceptional cases high numbers of fine asperities can be provided by abrasion of concretions that formed in coarse-grained substrates (*e.g.*, Loope *et al.*, 2012), or by differential cementation of original bedding. However, in deep-marine systems where striated grooves are common, mud clasts are abundant, and gravel-sized tools of non-mud composition, such as concretions, are rare in comparison (Peakall *et al*., 2020). Armoured mud clasts are therefore expected to be abundant in these settings and striated grooves may give a record of armoured mud clasts that were covered in sand grains. These clasts may be difficult to recognise in the deposits of many deep-water systems, given the restricted spatial variations in grain size that are often present within the sand fraction (*e.g.*, Jobe *et al*., 2012; Kane *et al*., 2017; Pierce *et al*., 2018), thus hindering the distinction between armour sediment and the main sediment in event beds. Examples of armoured mud clasts are known from modern (Gutmacher & Normark, 2002; Stevenson *et al*., 2018) and ancient (*e.g.*, Stanley, 1964; Mutti & Normark, 1987; Felix *et al*., 2009; Dodd *et al*., 2019; Privat *et al*., 2021; Jones *et al*., 2022; Scarselli, 2023) deep-water clastic systems, with tool diameters ranging from 0.05 m to 0.8 m (Stanley, 1964; Stevenson *et al*., 2018), and coatings ranging in size from medium- to coarse-grained siliciclastic and bioclastic sand to pebbles (Stanley, 1964; Chun *et al*., 2002; Privat *et al*., 2021). Armoured mud clasts are known to be far more resistant to breakage and abrasion than mud clasts without an armour (Hizzett *et al*., 2020) and thus stronger as cutting tools.

Given the apparent rarity of concretions with fine asperities, the known examples of armoured mud clasts, and the ubiquity of mudstone clasts in deep-marine clastic systems, it appears that the fine striae of striated grooves might in most cases reflect the transport of armoured mud clasts that have been incorporated into a debris flow, *i.e.*, a quasi-laminar plug flow (see discussion below). Examples of armoured mud clasts are known from both subaqueous debris flows (Chun *et al*., 2002) and hybrid events (Haughton *et al.*, 2003, 2009; Felix *et al*., 2009). This interpretation suggests that substantial numbers of striae in grooves indicate the presence of armoured mud clasts, and that the width of the striae can be used to estimate the roughness of the surficial mud clast coating. Armoured mud clasts may therefore be more prevalent in deep-water clastic systems than presently recognised.

A process model for the formation of chevrons and striated grooves

The present experiments demonstrate the importance of tools dragged in fixed positions through substrates with specific rheological properties for the formation of chevrons and striated grooves. The tool marks observed in the experiments are analogous to the pristinely preserved structures observed in the rock record (*e.g.*, Peakall *et al*., 2020). However, the paradox remains as to why a flow with cohesive strength that can transport and drag tools through the substrate, does not simultaneously erode the delicate structures, such as striae and chevrons, that are shown here to form in soft, ductile substrates. Existing knowledge of cohesive flow dynamics can be utilised to resolve this paradox. Quasi-laminar plug flows (debris flows) have been shown to possess a fluidal basal layer beneath the rigid plug (Fig. 9; Baas *et al*., 2009, 2011; Peakall *et al*., 2020). Tools, typically clasts, can be envisaged to protrude from the base of the plug flow where they are held in place by cohesive strength. The velocity of the plug flow is greater than that of the fluidal basal layer (Baas *et al*., 2009, 2011) and thus the tools move through this layer whilst being dragged through the substrate. The fluidal basal layer consists of two parts, a shear zone that exhibits minor residual turbulence, overlying a thickened viscous sublayer at the base of the flow where viscous forces suppress turbulence (Fig. 9). This viscous sublayer was 4–5% of the flow depth (*c.* 6 mm) in the experiments of Baas *et al*. (2009) and, whilst scaling relationships are unknown, Peakall *et al*. (2020) estimated that natural flows likely have viscous sublayers that are tens of millimetres thick, perhaps up to 100 mm. This model explains how tools being dragged through the bed, at velocities of *c.* 1 m s^{-1} (Peakall *et al*., 2020), can be spatially and temporally related to a near absence of erosion, and therefore the preservation of delicate, at times millimetric, structures in soft, ductile muds. The corollary of this contention is that such sole structures show that the formative flows consist of plug flows riding on a fluidal basal layer with a thickened viscous sublayer, rather than laminar plug flows (*sensu* Peakall *et al*., 2020), where the plug flow extends all the way to the base of the flow.

A second paradox is how the weakest substrates, such as those associated with cut chevrons, are not eroded by the head of the flow prior to the formation of the sedimentary structures. Research on the origin of grooves has argued that in some cases these may be formed by a debritic head (Baas *et al*., 2021), in keeping with observations from modern currents that the front of the flow has sediment concentrations that can be orders of magnitude higher than the rest of the flow (Azpiroz-Zabala *et al*., 2017; Pope *et al*., 2022). In such cases, it is argued that, as a result of a debritic head with an associated thickened viscous sublayer, there can be an absence of erosion of the soft substrate by turbulent or laminar flows. Thus, weak substrates are preserved and cut chevrons can be formed

within these. In other cases, such as chevron-less groove marks, the substrate is either more consolidated prior to the arrival of the flow, or the front of the flow was capable of eroding ('stripping off') the uppermost and weakest parts of the substrate prior to the formation of the chevrons, perhaps reflecting some ongoing fluid mixing, and associated erosion, at the front of a debritic head. The corollary of these processes is that chevron marks, and particularly cut chevron marks, are a likely indicator of flows that have debritic heads associated with no, or limited, erosion.

The presence of a fluidal basal layer and thickened viscous sublayer in natural quasi-laminar plug flows, and the associated protection of the bed from turbulence and erosion, also suggest that the absence of a flow in the present experiments likely does not cause the structures to develop and be preserved in a significantly different way to those in natural environments.

Is groove width a proxy for tool size?

The experimental data reveal a large variation in the width and depth of the groove marks (Figs 8A, B), suggesting that the value of using groove mark size as a proxy for the diameter of the formative tool is severely limited. This is confirmed by analysis of groove mark width and depth as calculated from the penetration depth of the spherical tool for each yield strength (Fig. 10). For all types of tool mark, groove width is equal to or smaller than the diameter of the tool and the groove depth is smaller than the radius of the tool (Figs 8A, B and 10). These differences are greatest for the cut chevron marks and chevron-less groove marks, because of rapid filling of the groove and shallow tool penetration depths, respectively. Only the groove widths of the interrupted chevron marks approach the tool diameter to within *c.* 7.5% (4 mm) at τ_y = 74.4 – 91.3 N m^{-2} (Fig. 8B). The implication is that groove width can only be used as an approximate representation of tool diameter for interrupted chevron marks, where the chevrons are long and wide relative to the groove width and the angle of the chevrons with respect to the flow direction is low (Fig. 8C). Groove width for all other types of tool mark, as well as the depth of all groove marks, can thus only be used as an indicator of minimum tool diameter.

Tool mark shape as a proxy for substrate yield stress

The present laboratory experiments reveal predictable relationships between tool mark shape and yield stress of kaolinite beds (Fig. 11), which allows the cohesive strength of the bed to be estimated from tool mark shape, with

support from tool mark size. The ranges in yield stress (Fig. 11) are within the fluid–solid category of van Rijn (1993) for all the tool mark types with chevrons, whereas groove marks without chevrons extend across the boundary from fluid–solid to firm mud. Moreover, tool marks do not form in fluid mud (at τ_y < 24.9 N m^{-2}), as defined in the classification scheme of van Rijn (1993). The predicted range of yield stresses of 58.9 to 158.0 N m^{-2} for the formation of cut and interrupted chevrons marks is remarkably small and may explain why chevron marks are less common in the geological record than chevron-less groove marks (Enos, 1969; Middleton & Hampton, 1973; Peakall *et al.*, 2020), which are inferred to form at yield stresses exceeding 158.0 N m^{-2}, including in stiff, and possibly hard, mud. The prominence of striae in groove marks may also be an additional qualitative measure to estimate yield stress of the bed at the time of striae formation.

In the present experiments, the weight of the tool determined the relative depth to which the tool penetrated the clay bed. However, in natural flows the tool is held at the base of the plug flow, and thus the weight applied to the substrate is that of the plug flow, relative to that of the fluidal basal layer (Fig. 9). In turn, the applied weight determines the depth of incision (Fig. 9), and thus the weight of the clast is not a key variable in controlling penetration depth. However, differences in the applied weight from the overlying plug flow will lead to different penetration depths and thus widths of the chevrons and striated grooves. Whilst penetration depths may vary relative to those observed in the present experiments, the same broad patterns of tool mark width and depth as a function of sole mark type (Fig. 11) and substrate strength are to be expected.

Preservation potential of tool marks

The preservation potential of tool mark types (Fig. 11) may vary with the rheological properties of the bed they are cut into. We postulate that tool marks in mud with a low water content, and thus high yield stress, have a higher preservation potential than those in mud with a high water content. In other words, cut and low-angle interrupted chevron marks in soft mud should possess a lower preservation potential than high-angle interrupted chevron marks, which in turn have a lower preservation potential than chevron-less groove marks formed in stiff mud. This provides further reasoning for the observation that groove marks are more common than chevron marks on the base of sediment beds (Enos, 1969; Middleton & Hampton, 1973; Peakall *et al.*, 2020). In deep-marine environments, yield stresses typical of soft substrates containing tool marks with chevrons (of the order of tens of N m^{-2}; Equation 4) can be overcome by turbidity currents laden with 5% sediment and travelling at 2 to 3 m s^{-1},

calculated using the quadratic stress law with a drag coefficient of 0.01 (Parker *et al.*, 1987). Turbidity currents with similar characteristics are common in the modern oceans (*e.g.*, Pope *et al.*, 2022), and thus they likely formed turbidites in the sedimentary record, implying that tool marks with chevrons may be preserved only under specific circumstances (Fig. 12). These include sites where: (a) the flow that forms the tool mark bypasses (*i.e.*, the equilibrium flows of Crisóstomo-Figueroa *et al.*, 2020) the location and there is an extended period without flow across the site afterwards (Peakall *et al.*, 2020; Baas *et al.*, 2021); (b) the seabed has sufficient time to consolidate, thus establishing the 'true substrates' of Davies & Shillito (2021); (c) there is lack of bioturbation, and; (d) the flow that casts the bed is solely depositional, and does not erode these delicate structures. Flow bypass is required because deposited sediment is expected to load into the fluid–solid and destroy any tool marks with chevrons. Bed consolidation leads to an increase in yield strength, thus aiding future tool mark preservation. In the classification scheme of van Rijn (1993), the time needed to progress from a fluid–solid to stiff mud, thereby increasing the preservation potential of the tool marks, is estimated to be of the order of years to decades (Table 2). Bed consolidation and strengthening would enable the substrate to support progressively thicker sand beds without undergoing liquefaction and loading. Consequently, the preservation potential of chevrons that form in the weakest substrates can be postulated to be higher under thinner beds that require shorter timescales between the formation of the sole structures, and subsequent deposition. However, field data to test this contention is currently absent. Furthermore, given their delicate nature, tool marks with chevrons will be destroyed by significant bioturbation, and hence their preservation potential should be greater during dysoxic and anoxic near-bed conditions, when bioturbation is restricted. Lastly, the flow that covers the bed, and casts the structures, needs to be solely depositional (i.e., no associated erosion). Such flows are common in turbiditic systems, associated with flat-based non-erosive sand overlying mud (*e.g.*, Walker & Mutti, 1973; Carlson & Grotzinger, 2001; Brooks *et al.*, 2018).

The dependence of tool mark characteristics upon substrate type, and particularly the narrow rheological range in which tool marks with chevrons form, also suggests that the abundance of such tool marks may have changed over geological time. A major change in seafloor ecology occurred during the Ordovician, with burrowing becoming more intense (Orr, 2001; Mángano *et al.*, 2016). Furthermore, the depth in the bed to which mixing generated by bioturbation occurs increased up to the late Silurian, where it attained a character matching modern conditions

(Tarhan, 2018). Thus, greater potential mixing depth and bioturbation intensity may have decreased substrate strength from the Ordovician onwards, thus favouring a higher frequency of tool marks with chevrons. Conversely, however, their preservation may have been hindered by enhanced bioturbation. Chevron-less grooves form over a wider range of firmer substrate rheology, and therefore are less likely to be affected by deposition and deformation immediately after formation, and would be less influenced by bioturbation. Nonetheless, the frequency of formation of different types of groove mark will likely have changed over time, with a greater frequency of harder substrates prior to the late Silurian, which would have favoured the production of chevron-less grooves.

In summary, the present experiments suggest that the preservation of tool marks with chevrons requires several conditions (Fig. 12): (1) a soft substrate in the fluid–solid category of van Rijn (1993) at a narrow range of yield stresses; (2) flow bypass; (3) a lack of bioturbation, perhaps encouraged by dysoxic or anoxic conditions; (4) sufficient time for bed consolidation, of the order of years to decades, and; (5) the succeeding flow to be dominantly depositional and unable to erode the chevron marks. Notwithstanding these requirements, the present experiments have shown predictable variations in tool mark shape that can be used to appraise bed densities and yield stresses, and thus bed erodibility and consolidation state, of deposits in the rock record at the time of tool mark formation (Fig. 11).

CONCLUSIONS

This study has explored the formative mechanisms of cut and interrupted chevron marks, and striated grooves, to investigate how these provide information on substrate rheology at the time of their formation. Cut chevron marks form in weak mud beds, as the substrate deforms in a fluid-like manner around a tool being dragged through the sediment, filling the groove behind it, and leaving just a narrow groove. The chevrons form by broader deformation to each side of the groove. Interrupted chevrons form in stronger substrates where the central groove is preserved. Striated grooves are likely largely the product of armoured mud clasts, with the depth and spacing of striae recording the roughness of the armouring grains. As substrate yield stress increases, there is a progression from no tool marks, to cut chevrons, interrupted chevrons, striated grooves with chevrons, and finally striated grooves without chevrons. The angle and width of chevron marks also varies with bed yield stress, with cut chevrons forming

in a narrow range of bed strengths characterised by a weak fluid–solid rheology. To preserve these delicate structures as sole marks on the base of sandstone beds, we postulate a time gap of the order of years to decades to produce bed consolidation and strengthening prior to deposition of the overlying sand. During this time, bioturbation needs to be absent or limited, perhaps implying anoxic or dysoxic conditions. This knowledge of sole mark type as a function of bed yield stress, can be inverted to interpret palaeosubstrate rheology from chevron and groove types, thus providing a new approach to determining the erodibility of the seabed in deep-marine systems dominated by sediment gravity flows. Combining these results with considerations of the extent of seafloor bioturbation, and its impact on substrate rheology, suggests that the abundance of these sole structures likely changed over geological time. Chevron-less grooves would have been favoured by the harder substrates present prior to the late Silurian. Chevron formation is more likely in weaker substrates, particularly post late-Silurian, although their preservation potential would also likely be lower as a result of enhanced bioturbation.

ACKNOWLEDGEMENTS

The experimental data presented herein were acquired by Dylan McGowan and Amisha Salian as part of the Bangor University Undergraduate Internship Scheme. The laboratory setup and consumables were funded by a research grant from Equinor, Norway. Will Taylor is thanked for his help with figure drafting. We also thank Associate Editor Kevin Taylor and Reviewers Lawrence Amy and Paul Myrow for their insightful comments that helped improve the paper.

The data that support the findings of the study are available from the corresponding author upon reasonable request.

REFERENCES

Allen, J.R.L. (1984) *Sedimentary Structures: Their Character and Physical Basis*. Elsevier, Amsterdam, 1256 pp.

Amos, C.L., Bergamasco, A., Umgiesser, G., Cappucci, S., Cloutier, D., DeNat, L., Flindt, M., Bonardi, M. and **Cristante, S.** (2004) The stability of tidal flats in Venice Lagoon—the results of in-situ measurements using two benthic, annular flumes. *Journal of Marine Systems*, **51**, 211–241.

Azpiroz-Zabala, M., Cartigny, M.J.B., Talling, P.J., Parsons, D.R., Sumner, E.J., Clare, M.A., Simmons, S.M., Cooper, C. and **Pope, E.L.** (2017). Newly recognized turbidity current structure can explain prolonged flushing of submarine canyons. *Science Advances*, **3**, e1700200.

Baas, J.H. and **Best, J.L.** (2002) Turbulence modulation in clay-rich sediment-laden flows and some implications for sediment deposition. *Journal of Sedimentary Research*, **72**, 336–340.

Baas, J.H., Best, J.L., Peakall, J. and **Wang, M.** (2009) A phase diagram for turbulent, transitional, and laminar clay suspension flows. *Journal of Sedimentary Research*, **79**, 162–183.

Baas, J.H., Best, J.L. and **Peakall, J.** (2011) Depositional processes, bedform development and hybrid flows in rapidly decelerated cohesive (mud-sand) sediment flows. *Sedimentology*, **58**, 1953–1987.

Baas, J.H., Tracey, N.D. and **Peakall, J.** (2021) Sole marks reveal deep-marine depositional process and environment: Implications for flow transformation and hybrid-event-bed models. *Journal of Sedimentary Research*, **91**, 986–1009.

Baker, M.L., Baas, J.H., Malarkey, J., Silva Jacinto, R., Craig, M.J., Kane, I.A. and **Barker, S.** (2017) The effect of clay type on the properties of cohesive sediment gravity flows and their deposits. *Journal of Sedimentary Research*, **87**, 1176–1195.

Benton, M.J. and **Gray, D.I.** (1981) Lower Silurian distal shelf storm-induced turbidites in the Welsh Borders: sediments, tool marks and trace fossils. *Journal of the Geological Society of London*, **138**, 675–694.

Bertram, V. (2000) *Practical Ship Hydrodynamics*. Butterworth-Heinemann, Oxford, 270 pp.

Beukes, N.J. (1996) Sole marks and combined-flow storm event beds in the Brixton Formation of the siliciclastic Archean Witwatersrand Supergroup, South Africa. *Journal of Sedimentary Research*, **66**, 567–576.

Boggs Jr, S. (2014) *Principles of Sedimentology and Stratigraphy, 5th Edition*. Pearson, Harlow, 564 pp.

Bridge, J.S. and **Demicco, R.V.** (2008) *Earth Surface Processes, Landforms and Sediment Deposits*. Cambridge University Press, Cambridge, 815 pp.

Brooks, H.L., Hodgson, D.M., Brunt, R.L., Peakall, J., Poyatos-Moré, M. and **Flint, S.S.** (2018) Disconnected submarine lobes as a record of stepped slope evolution over multiple sea-level cycles. *Geosphere*, **14**, 1753–1779.

Brooks, H.L., Ito, M., Zuchuat, V., Peakall, J. and **Hodgson, D.** (2022) Channel-lobe transition zone development in tectonically-active settings: Implications for hybrid bed development. *The Depositional Record*, **8**, 829–868.

Carlson, J. and **Grotzinger, J.P.** (2001) Submarine fan environment inferred from turbidite thickness distributions. *Sedimentology*, **48**, 1331–1351.

Chun, S.S., Choe, M.Y. and **Chough, S.K.** (2002) Armored mudstone boulders in submarine debris-flow deposits, the Hunghae Formation, Pohang Basin: An evidence for the large-scale slumping of adjacent area of a submarine channel or scar wall. *Geosciences Journal*, **6**, 215–225.

Collinson, J. and **Mountney, N.** (2019) *Sedimentary Structures, 4th Edition*. Dunedin Academic Press, Edinburgh, Scotland, 340 pp.

Collinson, J., **Mountney, N.** and **Thompson, D.** (2006) *Sedimentary Structures – 3rd edition*. Terra Publishing, Harpenden, England, 292 pp.

Craig, G.Y. and **Walton, E.K.** (1962) Sedimentary structures and palaeocurrent directions from the Silurian rocks of Kirkcudbrightshire. *Transactions of the Edinburgh Geological Society*, **19**, 100–119.

Crisóstomo-Figueroa, A., McArthur, A.D., Dorrell, R.M., Amy, L. and **McCaffrey, W.D**. (2021) A new modelling approach to sediment bypass prediction applied to the East Coast Basin, New Zealand. *Geological Society of America Bulletin*, **133**, 1734–1748.

Davies, N.S. and **Shillito, A.P.** (2021) True substrates: The exceptional resolution and unexceptional preservation of deep time snapshots on bedding surfaces. *Sedimentology*, **68**, 3307–3356.

Dodd, T.J.H., McCarthy, D.J. and **Richards, P.C.** (2019) A depositional model for deep-lacustrine, partially confined, turbidite fans: early Cretaceous, North Falkland Basin. *Sedimentology*, **66**, 53-80.

Draganits, E., Schlaf, J., Grasemann, B. and **Argles, T.** (2008) Giant submarine landslide grooves in the Neoproterozoic / Lower Cambrian Phe Formation, Northwest Himalaya: Mechanisms of formation and palaeogeographic implications. *Sedimentary Geology*, **205**, 126–141.

Dżułyński, S. (1996) Erosional and deformational structures in single sedimentary beds: a genetic commentary. *Annales Societatis Geologorum Poloniae*, **66**, 101–189.

Dżułyński, S. and **Sanders, J.E.** (1962) Current marks on firm mud bottoms. *Transactions of the Connecticut Academy of Arts and Sciences*, **42**, 57–96.

Dżułyński, S. and **Simpson, F.** (1966) Experiments on interfacial current markings. *Geologica Romana*, **5**, 197–214.

Dżułyński, S. and **Walton, E.K.** (1963) Experimental production of sole markings. *Transactions of the Edinburgh Geological Society*, **19**, 279–305.

Dżułyński, S. and **Walton, E.K.** (1965) *Sedimentary Features of Flysch and Greywackes*. Developments in Sedimentology 7, Elsevier, Amsterdam, 274 pp.

Enos, P. (1969) Anatomy of a flysch. *Journal of Sedimentary Petrology*, **39**, 680–723.

Felix, M., Leszczynzki, S., Slaczka, A., Uchman, A., Amy, L. and **Peakall, J.** (2009) Field expressions of the transformation of debris flows into turbidity currents, with examples from the Polish Carpathians and the French Maritime Alps. *Marine and Petroleum Geology*, **26**, 2011–2020.

Gutmacher, C.E. and **Normark, W.R.** (2002) Sur submarine landslide, a deep-water sediment slope failure. In: *Submarine Landslides: Selected Studies in the U.S. Exclusive Economic Zone* (Eds W.C. Schwab, H.J. Lee and D.C. Twichell), U.S. Geological Survey, Bulletin 2002, 158–166.

Hall, J. (1843) *Geology of New York, Part 4*, *Comprising the Survey of the Fourth Geological District*. Charles Van Benthuyson and Sons, Albany, 683 pp.

Haughton, P.D., Barker, S.P. and **McCaffrey, W.D.** (2003) 'Linked' debrites in sand-rich turbidite systems — origin and significance. *Sedimentology*, **50**, 459–482.

Haughton, P., Davis, C., McCaffrey, W. and **Barker, S.** (2009) Hybrid sediment gravity flow deposits classification, origin and significance. *Marine and Petroleum Geology*, **26**, 1900–1918.

Hillel, D. (2004) *Introduction to Environmental Soil Physics*. Amsterdam, Elsevier Academic Press, 494 pp.

Hizzett, J.L., Sumner, E.J., Cartigny, M.J.B. and **Clare, M.A.** (2020) Mud-clast armoring and its implications for turbidite systems. *Journal of Sedimentary Research*, **90**, 687–700.

Jobe, Z.R., Lowe, D.R. and **Morris, W.R.** (2012) Climbing-ripple successions in turbidite systems: depositional environments, sedimentation rates and accumulation times. *Sedimentology*, **59**, 867–898.

Jones, G.E.D., Welbon, A.I.F., Mohammadlou, H., Sakharov, A., Ford, J., Needham, T. and **Ottesen, C.** (2022) Complex stratigraphic fill of a small, confined syn-rift basin: an Upper Jurassic example from offshore mid-Norway. In: *Cross-Border Themes in Petroleum Geology II: Atlantic Margin and Barents Sea* (Eds D. Chiarella, S.G. Archer, J.A. Howell, C.A.-L. Jackson, H. Kombrink and S. Patruno), Geological Society, London, Special Publication, 495, 139–177.

Kane, I.A., Pontén, A.S.M., Vangdal, B., Eggenhuisen, J.T., Hodgson, D.M. and **Spychala, Y.T.** (2017). The stratigraphic record and processes of turbidity current transformation across deep-marine lobes. *Sedimentology*, **64**, 1236–1273.

Kelling, G., Walton, E.K. and **Simpson, F.** (2007) The contribution of Stanislaw Dżułyński to flysch sedimentology: A 'western' perspective. *Annales Societatis Geologorum Poloniae*, **77**, 93–103.

Lamb, M.P., Myrow, P.M., Lukens, C., Houck, K. and **Strauss, J.** (2008) Deposits from wave-influenced turbidity currents: Pennsylvanian Minturn Formation, Colorado, U.S.A. *Journal of Sedimentary Research*, **78**, 480–498.

Li, S., Li, S., Shan, X., Gong, C. and **Yu, X.** (2017) Classification, formation, and transport mechanisms of mud clasts. *International Geology Review*, **59**, 1609–1620.

Loope, D.B., **Kettler, R.M., Weber, K.A., Hinrichs, N.L.** and **Burgess, D.T.** (2012) Rinded iron-oxide concretions: Hallmarks of altered siderite masses of both early and late diagenetic origin. *Sedimentology*, **59**, 1769-1781.

Mángano, M.G., Buatois, L.A., Wilson, M. and **Droser, M.** (2016) The great Ordovician biodiversification event. In: *The Trace-Fossil Record of Major Evolutionary Events* (Eds M.G. Mángano and L.A. Buatois) Springer, Dordrecht, 127-156.

Middleton, G.V. and **Hampton, M.A.** (1973) Sediment gravity flows: Mechanics of flow and deposition. In: *Turbidites and Deep-water Sedimentation* (Eds G.V. Middleton and A.H. Bouma), SEPM Pacific Section short course, 1–38.

Mutti, E. and **Normark W.R.** (1987) Comparing examples of modern and ancient turbidite systems: Problems and concepts. In: *Marine Clastic Sedimentology: Concepts and Case Studies* (Eds J.K. Legget and G.G. Zuffa), Springer, Dordrecht, 1–38.

Myrow, P.M., Lukens, C., Lamb, M.P., Houck, K. and **Strauss, J.** (2008) Dynamics of a transgressive prodeltaic system: Implications for geography and climate within a Pennsylvanian intracratonic basin, Colorado, U.S.A. *Journal of Sedimentary Research*, **78**, 512–528.

Orr, P.J. (2001) Colonization of the deep-marine environment during the early Phanerozoic: The ichnofaunal record. *The Geological Journal*, **36**, 265–278.

Parker, G., Garcia, M., Fukushima, Y. and **Yu, W.** (1987) Experiments on turbidity currents over an erodible bed. *Journal of Hydraulic Research*, **25**, 123–147.

Pe-Piper, G. and **Piper, D.J.W.** (2020) Significance of the chemistry and morphology of diagenetic siderite in clastic rocks of the Mesozoic Scotian Basin. *Sedimentology*, **67**, 782-809.

Peakall, J., Best, J.L., Baas, J., Hodgson, D.M., Clare, M.A., Talling, P.J., Dorrell, R.M. and **Lee, D.R.** (2020) An integrated process-based model of flutes and tool marks in deep-water environments: implications for palaeohydraulics, the Bouma sequence, and hybrid event beds. *Sedimentology*, **67**, 1601–1666.

Philippe, A.M., Baravian, C., Imperor-Clerc, M., De Silva, J., Paineau, E., Bihannic, I., Davidson, P., Meneau, F., Levitz, P. and **Michot, L.J.** (2011) Rheo-SAXS investigation of shear-thinning behaviour of very anisometric repulsive disc-like clay suspensions. *Journal of Physics: Condensed Matter*, **23**, 194112.

Pierce, C.S., Haughton, P.D.W., Shannon, P.M., Pulham, A.J., Barker, S.P. and **Martinsen, O.J.** (2018) Variable character and diverse origin of hybrid event beds in a sandy submarine fan system, Pennsylvanian Ross Sandstone Formation, western Ireland. *Sedimentology*, **65**, 952–992.

Pope, E.L., Cartigny, M.J.B., Clare, M.A., Talling, P.J., Lintern, D.G., Vellinga, A., Hage, S., Açikalin, S., Bailey, L., Chapplow, N., Chen, Y., Eggenhuisen, J.T., Hendry, A., Heerema, C.J., Heijnen, M.S., Hubbard, S.M., Hunt, J.E., McGhee, C., Parsons, D.R., Simmons, S.M., Stacey, C.D. and **Vendettuoli, D.** (2022) First source-to-sink monitoring shows dense head controls sediment flux and runout in turbidity currents. *Science Advances*, **8**, eabj3220.

Postma, G., Lang, J., Hoyal, D.C., Fedele, J.J., Demko, T., Abreu, V. and **Pederson, K.H.** (2021) Reconstruction of bedform dynamics controlled by supercritical flow in the channel–lobe transition zone of a deep-water delta (Sant Llorenç del Munt, north-east Spain, Eocene). *Sedimentology*, **68**, 1674–1697.

Privat, A.M-L., Hodgson, D.M., Jackson, C.A-L., Schwarz, E. and **Peakall, J**. (2021) Evolution from syn-rift carbonates to early post-rift deep-marine intraslope lobes: the role of rift basin physiography on sedimentation patterns. *Sedimentology*, **68**, 2563–2605.

Scarselli, N. (2023) Exploring the predictive power of seismic geomorphology to assess sedimentary characteristics of gravity-flow deposits: examples from offshore East and West Africa reservoirs. In: *Seismic Geomorphology: Subsurface Analyses, Data Integration and Palaeoenvironment Reconstructions* (Eds A.M.W. Newton, K.J., Andresen, K.J. Blacker, R. Harding and E. Lebas), Geological Society, London, Special Publications, 525, https://doi.org/10.1144/SP525-2021-58

Stanley, D.J. (1964) Large mudstone-nucleus sandstone spheroids in submarine channel deposits. *Journal of Sedimentary Petrology*, **34**, 672–676.

Stevenson, C.J., Feldens, P., Georgiopoulou, A., Schönke, M., Krastel, S., Piper, D.J.W., Lindhorst, K. and **Mosher, D.** (2018) Reconstructing the sediment concentration of a giant submarine gravity flow. *Nature Communications*, **9**, 2616.

Tarhan, L.G. (2018) The early Paleozoic development of bioturbation — Evolutionary and geobiological consequences. *Earth Science Reviews*, **178**, 177-207.

van Rijn, L.C. (1993) *Principles of Sediment Transport in Rivers, Estuaries and Coastal Seas*. Amsterdam, Aqua Publications, 700 pp.

Walker, R.G. and **Mutti, E.** (1973) Part IV – Turbidite facies and facies associations. In: *Turbidites and Deep Water Sedimentation* (Eds G.V. Middleton and A.H. Bouma), SEPM Pacific Section short course, 119-158.

Winterwerp, J.C., van Kesteren, W.G.M., van Prooijen, B. and **Jacobs, W.** (2012) A conceptual framework for shear flow–induced erosion of soft cohesive sediment beds. *Journal of Geophysical Research: Oceans*, **117**, C10020.

Yong, R.N., Nakano, M. and **Pusch, R.** (2012) *Environmental Soil Properties and Behaviour*. London, CRC Press, 455 pp.

Table 1. Experimental parameters.

Run	Bed bulk density kaolinite (kg m^{-3})	Yield stress (N m^{-2})	Tool mark type	Chevrons?	Grooves?	Striae?	Predicted bed bulk density montmorillonite (kg m^{-3})
1	1367.7	50.0	none	-	-	-	1266.5
2	1404.7	69.1	1	yes	narrow	no	1269.3
3	1413.6	74.4	2	yes	yes	yes	1270.0
4	1422.4	79.9	2	yes	yes	yes	1270.8
5	1431.0	85.5	3	yes	yes	yes	1271.6
6	1439.5	91.3	3	yes	yes	yes	1272.5
7	1472.4	116.2	3	yes	yes	yes	1276.1
8	1503.5	143.7	3	yes	yes	yes	1280.2
9	1532.8	173.5	4	no	yes	yes	1284.5
10	1560.7	205.4	4	no	yes	yes	1289.2
11	1587.1	239.2	4	no	yes	yes	1294.1
12	1612.2	274.7	4	no	yes	yes	1299.3

Table 2. Clay-bed type classification scheme of van Rijn (1993), showing estimated bed yield stress.

Clay-bed type	Wet bulk densities (kg m^{-3})	Estimated yield stresses (N m^{-2})	Consolidation stage	Typical period of consolidation
Dilute fluid mud	1000–1050	0–0.021	Freshly consolidated	1 day
Bingham-type fluid mud	1050–1150	0.021–3.70	Weakly consolidated	1 week
Dense fluid mud	1150–1250	3.70–23.1	Medium consolidated	1 month
Fluid–solid	1250–1350	23.1–331	Highly consolidated	1 year
Stiff mud	1350–1400	331–515	Stiff solid	10 years
Hard mud	>1400	>515	Hard solid	100 years

Note: Estimated yield stresses are based on calculating the yield stress for the given bed density for each of kaolinite (a 'weak' clay) and montmorillonite (a 'strong' clay), and taking the average of the two; see text for further details.

VIDEO AND FIGURE CAPTIONS

Video 1. Example of tool mark formation experiment. Yield stress: 79.9 N m^{-2} (Run 4 in Table 1).

Fig. 1. Schematic diagram showing three different chevron types as seen in planform view (upper), and flow-parallel cross-section for uninterrupted chevrons (lower). Modified after Allen (1984).

Fig. 2. Field examples of continuous tool marks. (**A**) V-shaped, uninterrupted chevron marks (from experiments in plaster-of-Paris, Jagiellonian University, Kraków, Poland). Chevrons are *c.* 20 mm wide. (**B**) Cut chevron marks with a narrow groove, similar to the chevron marks formed at yields stresses between 58.9 N m^{-2} and 71.6 N m^{-2} in the

present study (Bude Formation, North Devon, UK). Scale bar is 20 mm long. (**C**) Interrupted chevron marks with short, high-angle chevrons, similar to the chevron marks formed at yields stresses between 82.8 N m^{-2} and 158.0 N m^{-2} in the present study (Cloridorme Formation, Gaspé Peninsula, Canada). Lens cap for scale. (**D**) Interrupted chevron marks with long, low-angle chevrons, similar to the chevron marks formed at yields stresses between 71.6 N m^{-2} and 82.8 N m^{-2} in the present study (Cloridorme Formation, Gaspé Peninsula, Canada). Lens cap for scale. (**E**) Chevron-less groove mark with distinct parallel striae, similar to the chevron marks formed at yield stresses between 158.0 N m^{-2} and 274.7 N m^{-2} in the present study (southern Poland). Yellow bar is 100 mm long.

Fig. 3. Left-hand tool mark: Interrupted chevron marks with downstream end of the ridges being steepest and folded over on itself. Right-hand tool mark: Chevron-less, striated groove mark. Flow was from top to bottom of image. Scale on top of card is in centimetres. Photograph kindly provided by Lauren Birgenheier, University of Utah.

Fig. 4. Schematic drawing of the experimental setup as seen in planform. Note that the bentonite bands represent a surficial layer of bentonite overlying the kaolin clay. The tool is dragged from right to left.

Fig. 5. Spikey, spherical tool (diameter = 0.052 m) used in the experiments.

Fig. 6. Principal types of experimental tool mark. (**A**) Cut chevron marks: Chevron marks with narrow, central, non-striated groove mark at yield stress τ_b = 69.1 N m^{-2}. (**B**) Low-angle interrupted chevron marks: Striated groove mark with pronounced chevron marks and surficial mud clasts at τ_b = 74.4 N m^{-2}. (**C**) Low-angle interrupted chevron marks: Striated groove mark with pronounced chevron marks and surficial mud clasts at τ_b = 79.9 N m^{-2}. (**D**) High-angle interrupted chevron marks: Striated groove mark with medium-angle chevron marks at τ_b = 85.5 N m^{-2}. (**E**) High-angle interrupted chevron marks: Striated groove mark with weakly developed chevron marks at τ_b = 116.2 N m^{-2}. (**F**) Chevron-less groove mark: Narrow striated groove mark without chevron marks at τ_b = 239.2 N m^{-2}.

Fig. 7. Cross-sectional profiles perpendicular to the direction of movement of the tool for different bed yield stresses. (**A**) Cut chevron mark; (**B, C**) Low-angle interrupted chevron marks; (**D–G**) High-angle interrupted chevron marks; (**H–J**) Chevron-less groove marks.

Fig. 8. Geometrical properties of the experimental tool marks as a function of bed yield stress. (**A**) Maximum groove mark depth (blue) and mean of maximum height of left-lateral and right-lateral ridges of groove marks (red). (**B**) Groove mark width. (**C**) Chevron angle with respect to tool dragging direction, where the blue vertical lines

represent the standard deviation of the mean and 90° signifies absence of chevrons. Vertical dashed lines and schematic drawings at top of figure refer to tool mark types (from left to right): cut chevron mark; low-angle interrupted chevron mark; high-angle interrupted chevron mark; chevron-less groove mark.

Fig. 9. Schematic model of a quasi-laminar debris flow with armoured mud clasts attached to the base of the plug and penetrating through the underlying fluidal basal layer (FBL) that has a thickened viscous sublayer (vsl). Pristine preservation of the delicate, often millimetric chevrons and striae, is achieved because the plug flow of the debris flow sits above a fluidal basal layer, the lower part of which is the thickened viscous sub-layer. Clasts attached to the base of the plug flow form grooves and chevrons as they are dragged through the bed, but otherwise turbulence from the flow does not reach the bed. The flow velocity is constant in the plug and rapidly decreases to zero from the top to base of the FBL. Modified after Peakall *et al.* (2020).

Fig. 10. Groove mark width and depth, as calculated from the observed penetration depth of the spherical tool, against bed yield stress. The tool diameter and radius are given for comparison. Vertical dashed lines and schematic drawings at top of figure refer to tool mark types (from left to right): cut chevron mark; low-angle interrupted chevron mark; high-angle interrupted chevron mark; chevron-less groove mark.

Fig. 11. Conceptual model of tool mark type in relation to substrate yield stress.

Fig. 12. Preservation mechanism of cut chevron marks. A prolonged period of quiescence and anoxia or dysoxia, followed by deposition of sand from, for example, a turbidity current is required to preserve these tool marks in natural environments. A similar model applies to low-angle interrupted chevron marks, which also form in mud with a soft fluid–solid rheology (van Rijn, 1993). Note that striae caused by asperities, such as those on armoured mud clasts, do not show in cut chevron marks. Hence, smooth clasts, rather than the armoured clast shown in the left-hand drawing, would produce the same type of chevron marks.

Table 1. Experimental parameters.

Run	Bed bulk density kaolinite (kg m^{-3})	Yield stress (N m^{-2})	Tool mark type	Chevrons?	Grooves?	Striae?	Predicted bed bulk density montmorillonite (kg m^{-3})
1	1367.7	50.0	none	-	-	-	1266.5
2	1404.7	69.1	1	yes	narrow	no	1269.3
3	1413.6	74.4	2	yes	yes	yes	1270.0
4	1422.4	79.9	2	yes	yes	yes	1270.8
5	1431.0	85.5	3	yes	yes	yes	1271.6
6	1439.5	91.3	3	yes	yes	yes	1272.5
7	1472.4	116.2	3	yes	yes	yes	1276.1
8	1503.5	143.7	3	yes	yes	yes	1280.2
9	1532.8	173.5	4	no	yes	yes	1284.5
10	1560.7	205.4	4	no	yes	yes	1289.2
11	1587.1	239.2	4	no	yes	yes	1294.1
12	1612.2	274.7	4	no	yes	yes	1299.3

Table 2. Clay-bed type classification scheme of van Rijn (1993), showing estimated bed yield stress.

Clay-bed type	Wet bulk densities (kg m^{-3})	Estimated yield stresses (N m^{-2})	Consolidation stage	Typical period of consolidation
Dilute fluid mud	1000–1050	0–0.021	Freshly consolidated	1 day
Bingham-type fluid mud	1050–1150	0.021–3.70	Weakly consolidated	1 week
Dense fluid mud	1150–1250	3.70–23.1	Medium consolidated	1 month
Fluid–solid	1250–1350	23.1–331	Highly consolidated	1 year
Stiff mud	1350–1400	331–515	Stiff solid	10 years
Hard mud	>1400	>515	Hard solid	100 years

Note: Estimated yield stresses are based on calculating the yield stress for the given bed density for each of kaolinite (a 'weak' clay) and montmorillonite (a 'strong' clay), and taking the average of the two; see text for further details.

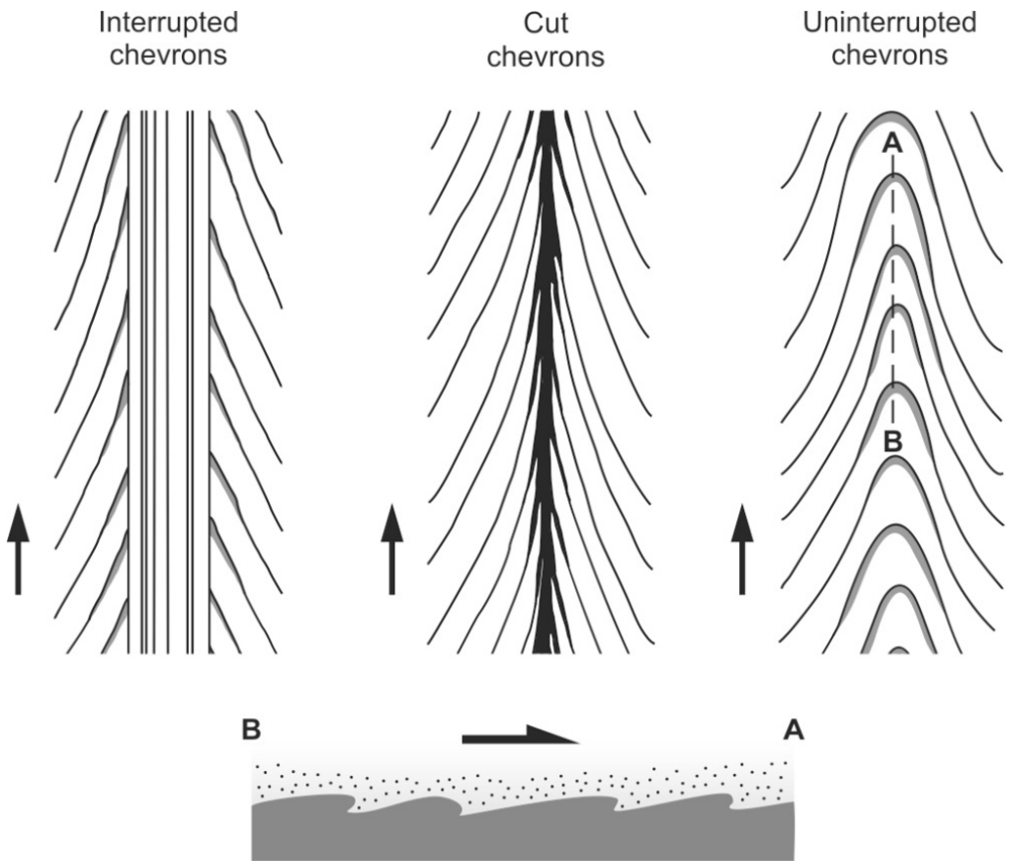

Schematic diagram showing three different chevron types as seen in planform view (upper), and flow-parallel cross-section for uninterrupted chevrons (lower). Modified after Allen (1984).

114x97mm (220 x 220 DPI)

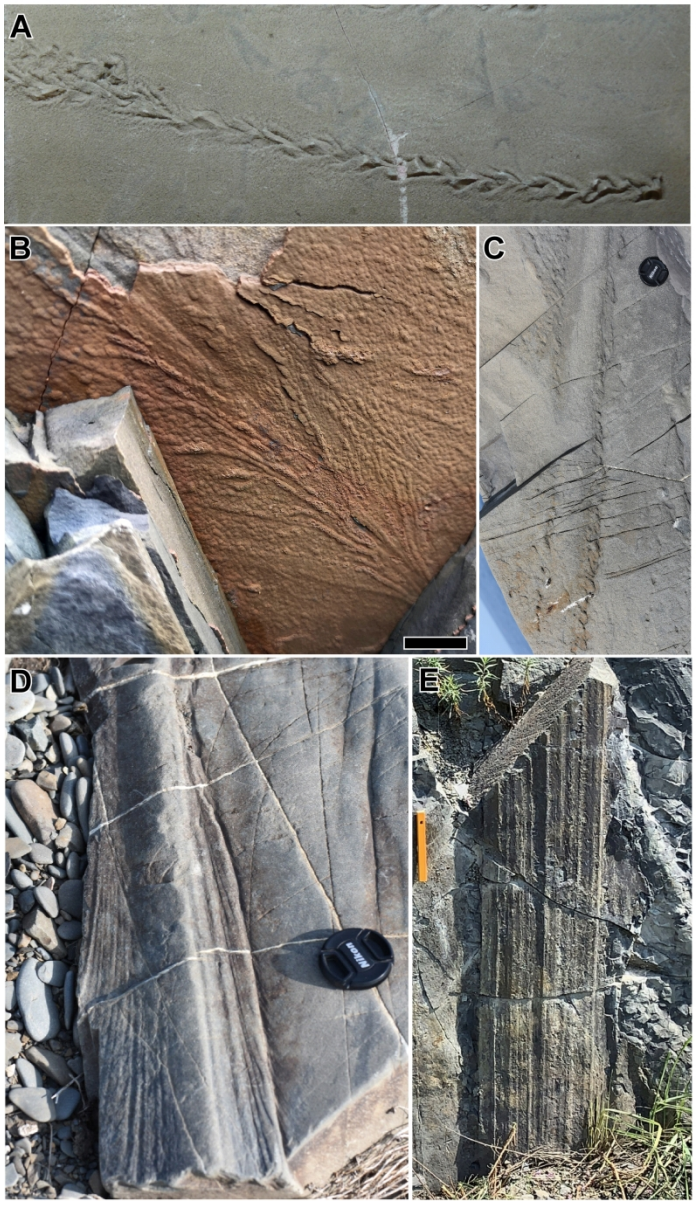

Field examples of continuous tool marks. (A) V-shaped, uninterrupted chevron marks (from experiments in plaster-of-Paris, Jagiellonian University, Kraków, Poland). Chevrons are c. 20 mm wide. (B) Cut chevron marks with a narrow groove, similar to the chevron marks formed at yields stresses between 58.9 N m^{-2} and 71.6 N m^{-2} in the present study (Bude Formation, North Devon, UK). Scale bar is 20 mm long. (C) Interrupted chevron marks with short, high-angle chevrons, similar to the chevron marks formed at yields stresses between 82.8 N m^{-2} and 158.0 N m^{-2} in the present study (Cloridorme Formation, Gaspé Peninsula, Canada). Lens cap for scale. (D) Interrupted chevron marks with long, low-angle chevrons, similar to the chevron marks formed at yields stresses between 71.6 N m^{-2} and 82.8 N m^{-2} in the present study (Cloridorme Formation, Gaspé Peninsula, Canada). Lens cap for scale. (E) Chevron-less groove mark with distinct parallel striae, similar to the chevron marks formed at yields stresses between 158.0 N m^{-2} and 274.7 N m^{-2} in the present study (southern Poland). Yellow bar is 100 mm long.

187x324mm (300 x 300 DPI)

Left-hand tool mark: Interrupted chevron marks with downstream end of the ridges being steepest and folded over on itself. Right-hand tool mark: Chevron-less, striated groove mark. Flow was from top to bottom of image. Scale on top of card is in centimetres. Photograph kindly provided by Lauren Birgenheier, University of Utah.

1422x1066mm (72 x 72 DPI)

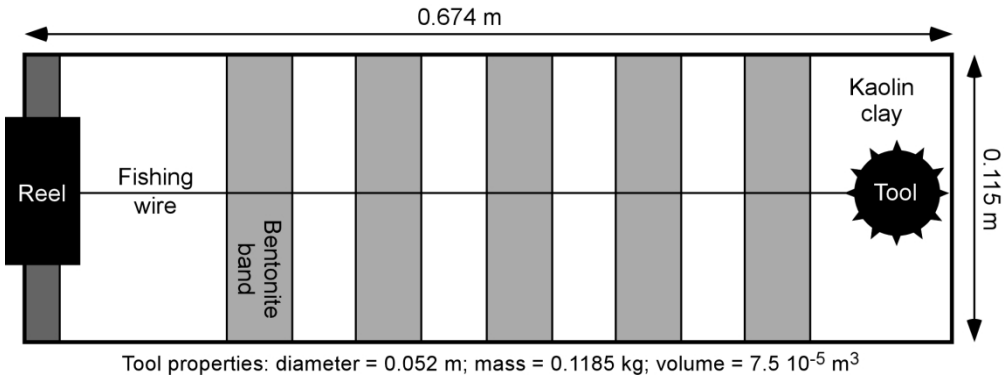

Schematic drawing of the experimental setup as seen in planform. Note that the bentonite bands represent a surficial layer of bentonite overlying the kaolin clay. The tool is dragged from right to left.

180x67mm (300 x 300 DPI)

Spikey, spherical tool (diameter = 0.052 m) used in the experiments.

173x171mm (72 x 72 DPI)

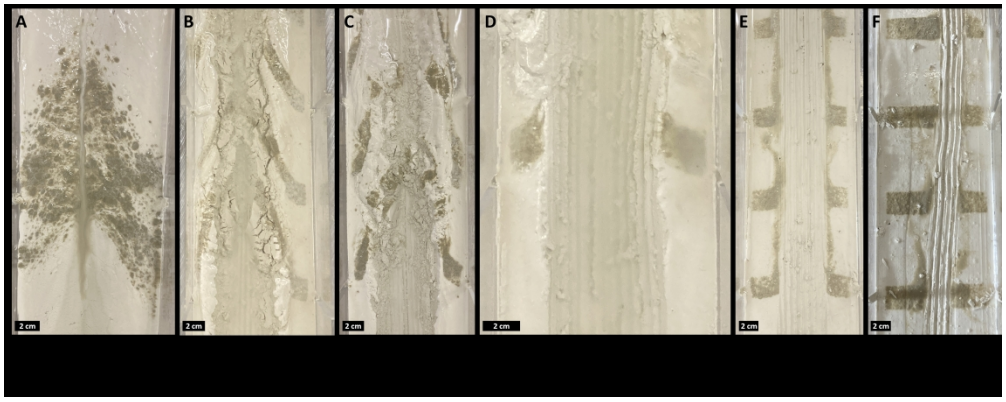

Principal types of experimental tool mark. (A) Cut chevron marks: Chevron marks with narrow, central, non-striated groove mark at yield stress τ b = 69.1 N m^{-2}. (B) Low-angle interrupted chevron marks: Striated groove mark with pronounced chevron marks and surficial mud clasts at τ b = 74.4 N m^{-2}. (C) Low-angle interrupted chevron marks: Striated groove mark with pronounced chevron marks and surficial mud clasts at τ b = 79.9 N m^{-2}. (D) High-angle interrupted chevron marks: Striated groove mark with medium-angle chevron marks at τ b = 85.5 N m^{-2}. (E) High-angle interrupted chevron marks: Striated groove mark with weakly developed chevron marks at τ b = 116.2 N m^{-2}. (F) Chevron-less groove mark: Narrow striated groove mark without chevron marks at τ b = 239.2 N m^{-2}.

335x131mm (330 x 330 DPI)

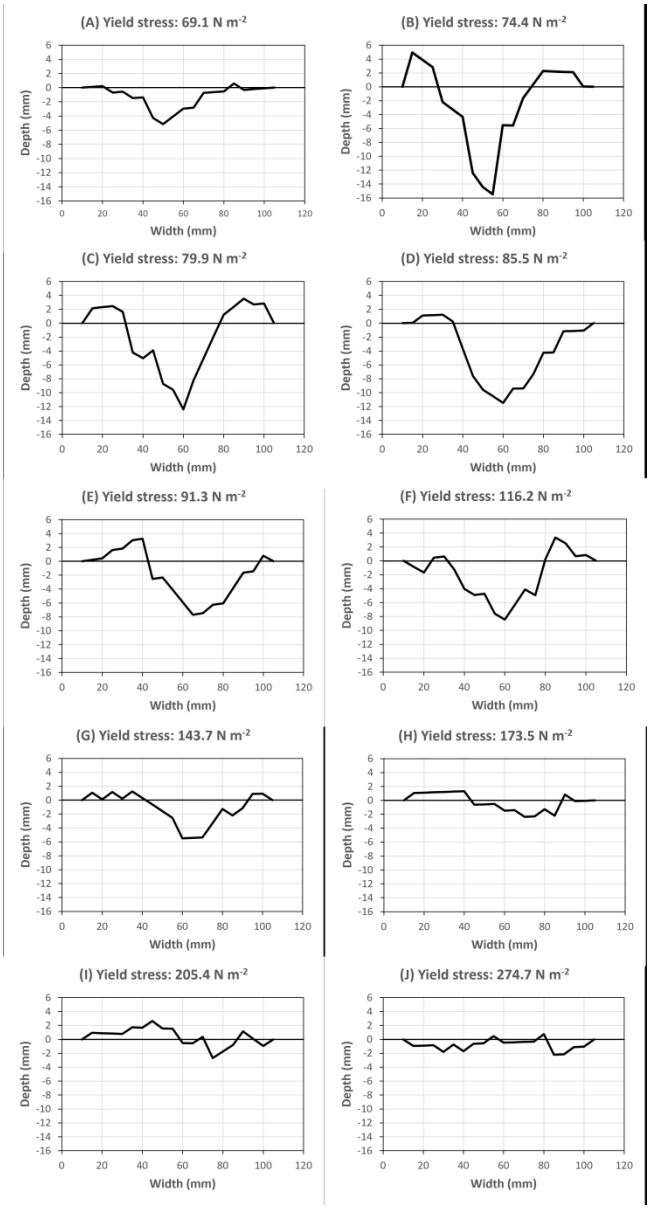

Cross-sectional profiles perpendicular to the direction of movement of the tool for different bed yield stresses. (A) Cut chevron mark; (B, C) Low-angle interrupted chevron marks; (D–G) High-angle interrupted chevron marks; (H–J) Chevron-less groove marks.

207x386mm (330 x 330 DPI)

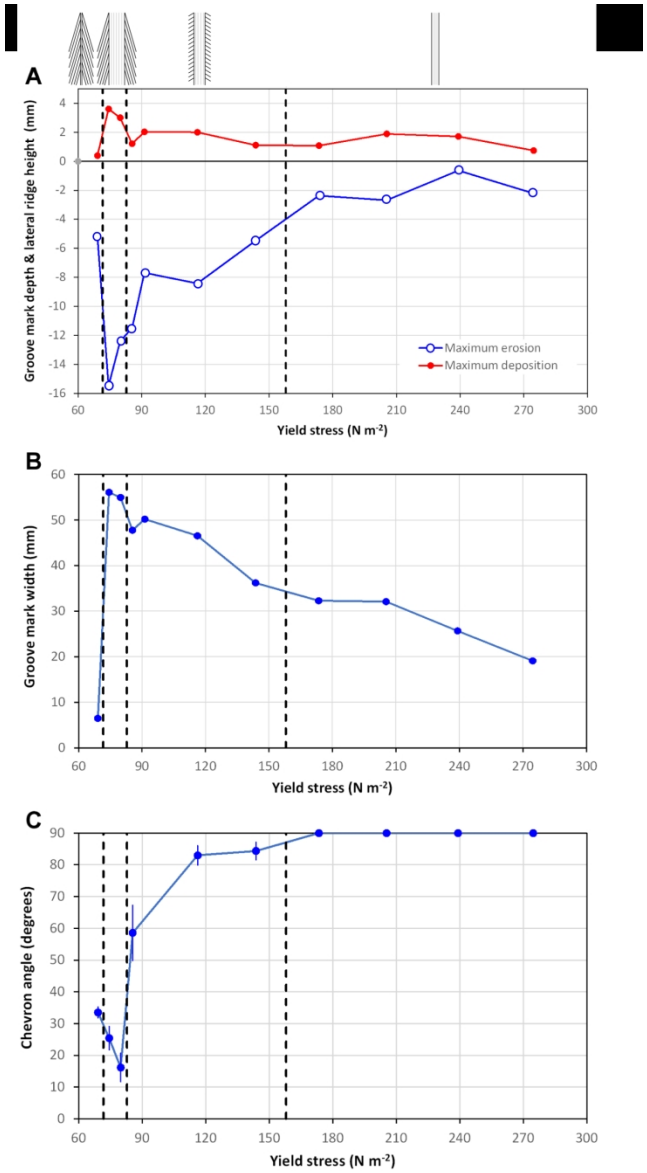

Geometrical properties of the experimental tool marks as a function of bed yield stress. (A) Maximum groove mark depth (blue) and mean of maximum height of left-lateral and right-lateral ridges of groove marks (red). (B) Groove mark width. (C) Chevron angle with respect to tool dragging direction, where the blue vertical lines represent the standard deviation of the mean and 90° signifies absence of chevrons. Vertical dashed lines and schematic drawings at top of figure refer to tool mark types (from left to right): cut chevron mark; low-angle interrupted chevron mark; high-angle interrupted chevron mark; chevron-less groove mark.

104x195mm (330 x 330 DPI)

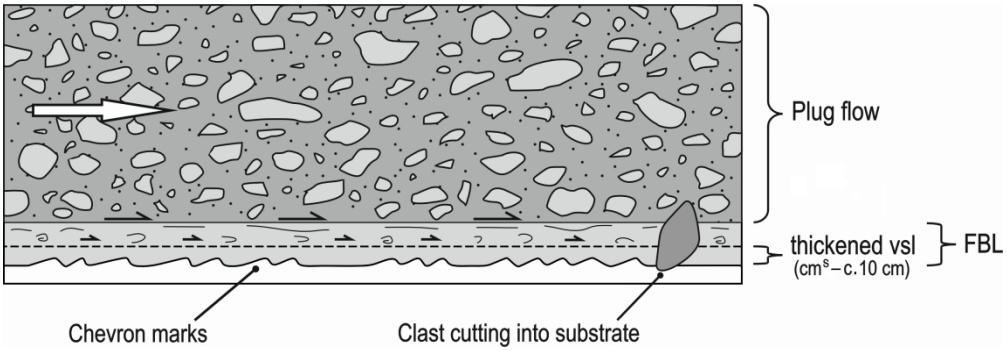

Schematic model of a quasi-laminar debris flow with armoured mud clasts attached to the base of the plug and penetrating through the underlying fluidal basal layer (FBL) that has a thickened viscous sublayer (vsl). Pristine preservation of the delicate, often millimetric chevrons and striae, is achieved because the plug flow of the debris flow sits above a fluidal basal layer, the lower part of which is the thickened viscous sub-layer. Clasts attached to the base of the plug flow form grooves and chevrons as they are dragged through the bed, but otherwise turbulence from the flow does not reach the bed. Modified after Peakall et al. (2020).

750x257mm (96 x 96 DPI)

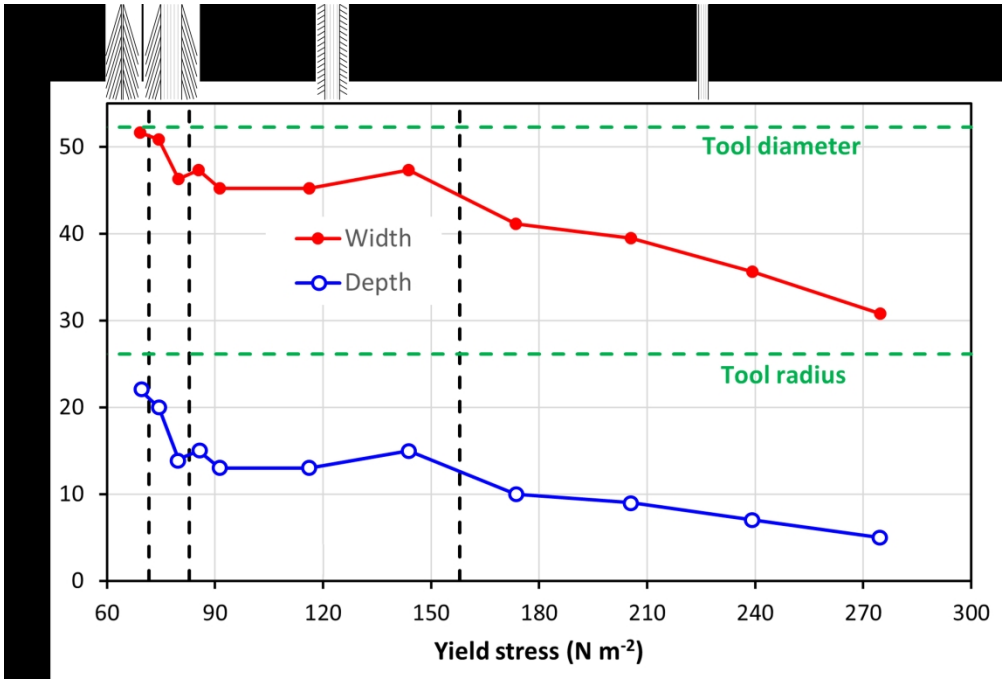

Groove mark width and depth, as calculated from the observed penetration depth of the spherical tool, against bed yield stress. The tool diameter and radius are given for comparison. Vertical dashed lines and schematic drawings at top of figure refer to tool mark types (from left to right): cut chevron mark; low-angle interrupted chevron mark; high-angle interrupted chevron mark; chevron-less groove mark.

246x166mm (330 x 330 DPI)

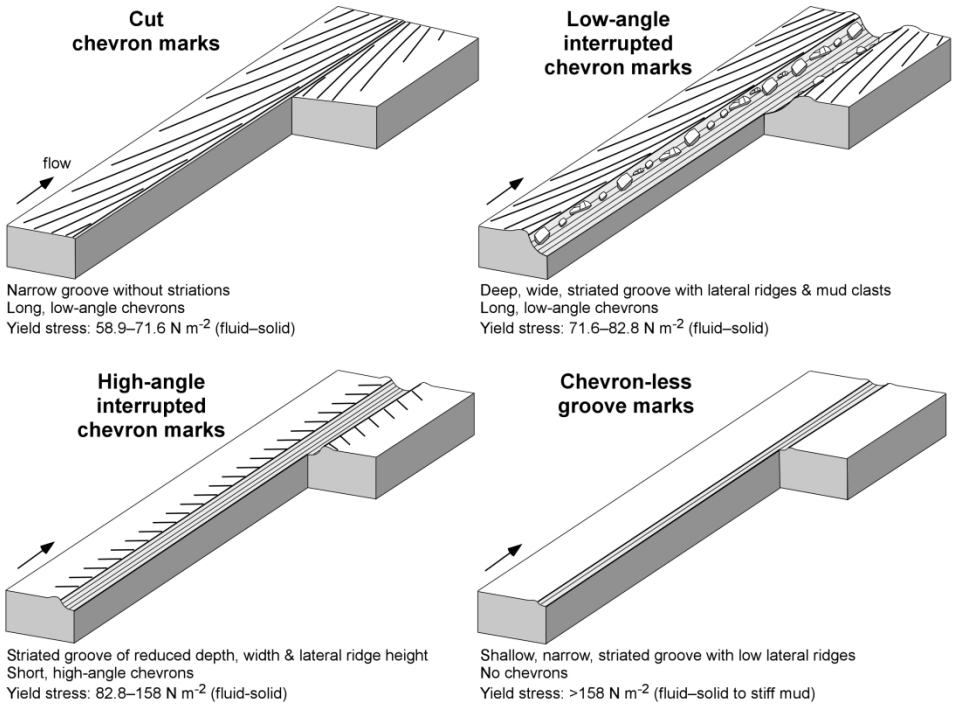

Conceptual model of tool mark type in relation to substrate yield stress.

269x188mm (300 x 300 DPI)

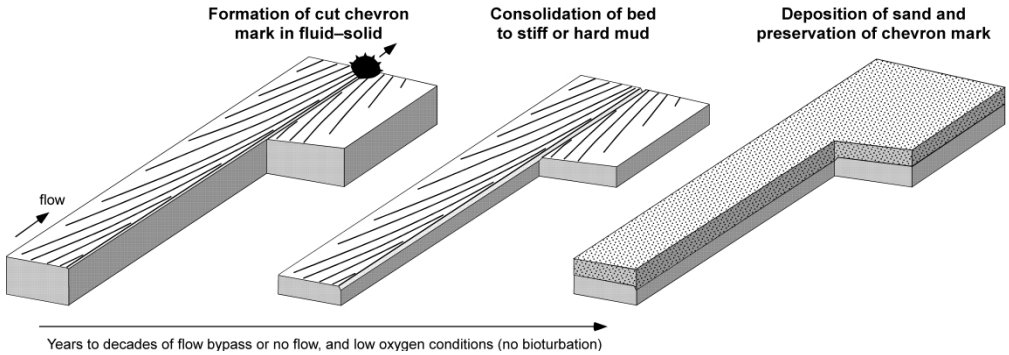

Preservation mechanism of cut chevron marks. A prolonged period of quiescence and anoxia or dysoxia, followed by deposition of sand from, for example, a turbidity current is required to preserve these tool marks in natural environments. A similar model applies to low-angle interrupted chevron marks, which also form in mud with a soft fluid–solid rheology (van Rijn, 1993). Note that striae caused by asperities, such as those on armoured mud clasts, do not show in cut chevron marks. Hence, smooth clasts, rather than the armoured clast shown in the left-hand drawing, would produce the same type of chevron marks.

295x102mm (600 x 600 DPI)